Chemical Engineering Research and Design 205 (2024) 486–497

Contents lists available at ScienceDirect

Chemical Engineering Research and Design

journal homepage: www.elsevier.com/locate/cherd

Fluid dynamics and mixing in a novel intermittently rotating bioreactor for CAR-T cell therapy: Spin-down from incomplete spin-up

G.G. Atanasova [a], A. Ducci [b], M. Micheletti [a,*]

[a] Dept. of Biochemical Engineering, University College London, Gower Street, London WC1E 6BT, UK
[b] Dept. of Mechanical Engineering, University College London, Gower Street, London WC1E 7JE, UK

ARTICLE INFO

Key words:
CliniMACS prodigy®
Intermittent agitation
Mixing without an impeller
Taylor-görtler instabilities
CAR-T manufacturing

ABSTRACT

This work explores the fluid flow and mixing within a new type of intermittently rotating bioreactor used for the automated manufacturing of CAR-T cell therapy products; CAR-T is a novel cell-based gene therapy which offers a single-dose cure for several forms of advanced blood cancer. The rotating cylinder bioreactor has a free surface and a liquid height to radius ratio of 0.5. Agitation is achieved via intermittent rotation of the entire vessel around its central vertical axis. No comprehensive engineering characterisation of the fluid dynamics in a bioprocessing context exists to date for this type of bioreactor. The present study examines the fluid dynamics and mixing during spin-down to rest following incomplete spin-up (i.e. the starting state of the fluid is not solid body rotation). Novel Particle Image Velocimetry (PIV) and Planar Laser-Induced Fluorescence (PLIF) data is presented, shedding light on the different transient flow regions inside the intermittently rotating bioreactor, and on the impact spin-up time has on the mixing efficiency of the subsequent spin-down stage. The results presented can be used to inform the design of a custom intermittent agitation pattern for any resembling cylinder bioreactors, the adoption of which could lead to higher yields and reduced costs for the cell expansion step of the manufacturing process.

1. Introduction

Advanced Therapy Medicinal Products (ATMPs) represent the cutting-edge frontier of medicine, offering potential cures for previously untreatable diseases. Among these Chimeric Antigen Receptor (CAR) T-cell therapy is a personalised cell-based gene therapy which provides a single-dose cure for multiple types of advanced blood cancer. Since the regulatory approval of the first two such commercial products in 2017, four more CAR-T cell therapies have been granted marketing authorisation, with hundreds of candidates currently undergoing clinical trials (Gustafson et al. 2022; Cappell and Kochenderfer, 2023).

Nevertheless, the difficulty in scaling up the production of CAR-T cell therapy remains due to the complexity and sensitivity of the process to various parameters. Changes in these parameters can unexpectedly impact the quality, safety, and effectiveness of the final product (Moutsatsou et al., 2019; El-Khazragy et al., 2020). Moreover, the process is labour-intensive and dependent on donor variability, thus leading to significant costs and insufficient supply of these life-saving medicines and emphasising the need for technological improvement and automation.

The automation of one or more of the steps of the CAR-T manufacturing process has been the focus of recent development in this area. Several commercial platforms are available, such as the CliniMACS Prodigy® (Miltenyi Biotec), Cocoon® (Lonza), and the G-Rex® (Scale Ready), with more platforms currently in development (e.g. by Ori Biotech or by Cellares). Of particular interest to the present work is the CliniMACS Prodigy®, which is a closed, fully automated system that can accommodate the whole bioprocess from starting materials to end product (Mock et al. 2016; Zhu et al. 2018; Alzubi et al. 2021). Its multifunctionality relies on the design of the CentriCult™ chamber, which serves both as a bioreactor and as a centrifuge, with a maximum working volume of 300 mL (75 % capacity) (Richter, 2014).

The CentriCult™ bioreactor features an unconventional geometry and intermittent agitation. Unlike traditional stirred-tank reactors (STRs), the CentriCult™ does not use traditional mixing equipment (i.e., impeller, sparger, or baffles), but instead the entire cylinder rotates intermittently around its central vertical axis to homogenise the cell culture. As the rotation rate of the bioreactor is started, stopped or reversed (spin-up, spin-down or spin-over), a distinct transient secondary flow is produced.

There exist several types of axisymmetrically rotating cylindrical

* Corresponding author.
E-mail address: m.micheletti@ucl.ac.uk (M. Micheletti).

https://doi.org/10.1016/j.cherd.2024.04.016
Received 18 December 2023; Received in revised form 3 April 2024; Accepted 10 April 2024
Available online 16 April 2024

Nomenclature

Greek symbols

$\Phi_\Theta{}^-$	Negative instantaneous tangential flux [-]
$\Phi_\Theta{}^+$	Positive instantaneous tangential flux [-]
Ω	Cylinder rotation rate [rad/s]
Ω'	Cylinder angular acceleration/deceleration [rad/s^2]
$\overline{\Phi}_\theta$	Time-averaged normalised tangential flux [-]
Φ_θ	Instantaneous normalised tangential flux [-]
γ_M	Fraction of mixed pixels [-]
θ	Angular coordinate rad
ν	Kinematic viscosity [m^2/s]
$\overline{\omega}$	Angular velocity of the fluid core during spin-down to rest from SBR [rad/s]
$\dot{\omega}_\theta$	Instantaneous space-averaged tangential vorticity of the T-G vortices after selection [s^{-1}]
$\overline{\omega}_\theta$	Time-averaged tangential vorticity [s^{-1}]
ω_θ	Instantaneous tangential vorticity [s^{-1}]

Roman symbols

b	Normalised pixel brightness [-]
e	Natural exponent [-]
Fr	Froude number [-]
g	Gravitational acceleration [m/s^2]
L	Liquid height at rest [m]
N	Rotation speed [rps]
r	Radial coordinate [m]
R	Cylinder radius [m]
r^*	Radial position of the propagating vertical shear front during spin-up [m]
Re	Reynolds number [-]
Re_{crit}	Critical Re for the onset of instabilities (instability type depends on context) [-]
t	Dimensional time [s]
T	Ekman time [-]
T_M	Ekman macromixing time [-]
t_M	Dimensional macromixing time [s]
t_{SU}	Spin-up time before the rotation is stopped and the resulting spin-down stage is studied [s]
T_{SU}	Spin-up Ekman time before the rotation is stopped and the resulting spin-down stage is studied [-]
t_U	Dimensional time required for the completion of spin-up [s]
T_U	Ekman time required for the completion of spin-up [-]
u_r	Radial components of the velocity [m/s]
u_θ	Tangential component of the velocity [m/s]
u_z	Axial component of the velocity [m/s]
z	Axial coordinate [m]

bioreactors that achieve mixing without an impeller or other conventional mixing equipment. The base-driven bioreactor, utilised for cultivating cartilage and bone constructs on an immobilized scaffold in the media, involves a partially filled vertical cylinder with a rotating flat base disc and a stationary sidewall. Cogan et. al. (2011) studied its secondary flow patterns computationally in a bioprocessing context, while Dusting et. al. (2006) experimentally analysed these using Stereoscopic Particle Image Velocimetry (SPIV). The convective Ekman flow and recirculating fluid within vortex breakdown bubbles (VBBs) create a low-shear, uniform, and controllable mixing environment Dusting et. al. (2006). Another example is the Taylor-Couette bioreactor, used for stem cell differentiation and growing tissue constructs (Chaudhuri and Al-Rubeai, 2005), which consists of two vertical coaxial cylinders with a narrow gap in between, filled with cell culture media. In the context of bioreactor technology and bioprocessing, it is worth to mention the works of Saini and Wick (2003, 2004), who demonstrated that the laminar Couette flow, established when the outer cylinder rotates and the inner is stationary, provides an easily controllable dissolved-oxygen environment, suitable for culturing cartilage constructs, and that of Curran and Black (2004, 2005) who showed that the Taylor-vortex flow regimes, induced by rotating the inner cylinder, while keeping the outer stationary, offer improved cell suspension and oxygen mass transfer, albeit at the expense of higher shear stress.

While the bioreactor design considered in this work is novel in a bioprocessing context, fluid dynamics theory for single vertically oriented rotating cylinders has been established for devices used in various other applications, such as ballistics (Goller and Ranov, 1968), aerospace engineering (Floryan, 1991) oceanography (Munk, 2001), and turbomachinery (Lopez et al., 2009). For the flow in a rotating cylinder, it is commonly accepted to use the definition of the Reynolds number, Re, employed for the flow over a finite rotating disc (Greenspan, 1968), which is shown in Eq. 1:

$$\mathrm{Re} = \frac{\Omega R^2}{\nu} \tag{1}$$

where Ω is the angular velocity of a cylinder of radius, R, rotating about its vertical axis, and ν is the kinematic viscosity of the fluid. The flow

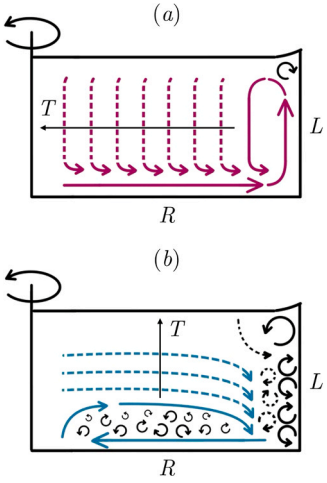

Fig. 1. Schematic representation of the secondary flow during a) spin-up from rest and b) spin-down from solid body rotation. The core flow is illustrated with magenta and cyan, in a) and b) respectively, and the Taylor-Görtler vortices in b) are shown by the sidewall in black, and other forms of instabilities in the endwall boundary layer, also in black. The flow is illustrated at an early time with solid contours, and dashed symbols indicate an arbitrarily later moment in time, as indicated by the arrows (adapted from Atanasova et al. 2023).

remains laminar for $Re < 3 \times 10^5$ (Schlichting and Gersten, 2017).

Greenspan and Howard (1963) and Wedemeyer (1964) laid the theoretical foundation for the flow in an impulsively accelerated completely filled cylinder (i.e. spin-up from rest). They showed that shortly after the instantaneous start of rotation, a viscous boundary layer of the von Kármán type develops at the bottom endwall and a Stewartson type boundary layer at the sidewall, where mass transfer occurs, while the interior of the fluid remains inviscid. The Ekman layer at the endwall expels fluid radially outward, and the radial outflow is balanced by an inflow from the interior, closing the Ekman circulation loop. A

schematic representation of the flow during spin-up can be found in Fig. 1a, adapted from Atanasova et al. (2023). A similar Ekman pumping was observed in the base-driven bioreactor, studied by Dusting et al. (2006) and Cogan et al. (2011) and was identified as a beneficial factor for convective mixing. Wedemeyer (1964) showed that spin-up is completed on the Ekman convection timescale, shown in Eq. 2:

$$T = t \times \left(\frac{\nu\Omega}{H^2}\right)^{\frac{1}{2}} = \Omega t \times \frac{R}{H} \times \frac{1}{\sqrt{\mathrm{Re}}}, \tag{2}$$

where T is the Ekman time, t is the dimensional time, and H is the height of a completely filled cylinder. The characteristic for spin-up vertical shear front of tangential velocity propagates radially inward from the sidewall to the axis of rotation, as depicted in the schematic in Fig. 1a, and its radial position, r^*, in Ekman time, T, is described by an exponential decay law as shown in Eq. 3:

$$\frac{r^*}{R} = e^{-bT} \tag{3}$$

Homicz and Gerber (1987), Choi et al. (1989, 1991) and Goller and Ranov (2013) extended the theory for completely filled cylinders to cylinders with a free surface. They performed computations and Laser Doppler Anemometry (LDA) experiments to characterise the tangential component of the velocity in a partially filled cylinder (free surface height to radius ratio, L/R = 1–2), undergoing spin-up from rest and showed that, provided that the free surface does not intersect the bottom or top endwalls of the cylinder, the characteristic spin-up timescale, characterised by the propagation of the vertical tangential velocity shear front, is still described by an exponential decay law as shown in Eq. 3. O'Donnell and Linden (1991) and Kloosterziel and Van Heijst (1992) performed experiments with tracer particles floating on the free surface of a cylinder, impulsively accelerated from rest, and showed that the characteristic dimensionless (Ekman) spin-up timescale increases with the Froude number, Fr, shown in Eq. 4, indicating that spin-up is slowed down by the increasing influence of the deforming free surface on the flow.

$$Fr = \frac{\Omega^2 R^2}{gL} \tag{4}$$

where g is the gravitational acceleration and L is the liquid height at rest. When the entire fluid has attained the angular velocity of the cylinder, its motion is defined as solid body rotation (SBR).

For small changes in the rotation rate, the problem of spin-down is essentially the same as that of spin-up, however, spin-down to rest is significantly different. When the rotation rate of the cylinder is impulsively brought to rest, the endwall boundary layer formed is of the Bödewadt type, characterised by a radial inflow along the endwall balanced by an axial efflux from the endwall boundary layer into the inviscid interior above it (Duck and Foster, 2001). This generates a similar pumping mechanism to spin-up but in the opposite direction, as illustrated in the schematic in Fig. 1b. The main difference between spin-up from rest and spin-down to rest arises from the action of the sidewall boundary layer. Due to the curvature of the sidewall, the decelerating flow in its vicinity, during spin-down to rest from SBR, causes the sidewall boundary layer to become unstable and take the form of counter-rotating vortex pairs, known as Taylor-Görtler (T-G) vortices, shown in green in the schematic in Fig. 1b. These vortices are a type of centrifugal instability which occurs when $Re > Re_{crit}$, where Re_{crit} varies in the literature between $140 < Re_{crit} < 320$ (Neitzel and Davis, 1981; Mathis and Neitzel, 1985; Cui, 2004; Kim and Choi, 2006). At the time of their onset, T-G vortices are identical to the Taylor vortices formed in the Taylor-Couette bioreactor, in which when the outer wall is stationary and the inner rotating, they are the primary mechanism through which micromixing is achieved (Curran and Black, 2004; Dusting and Balabani, 2009).

Euteneuer (1968, 1972) experimentally studied the T-G vortices during spin-down to rest from SBR in a completely filled transparent single cylinder with height to radius aspect ratio, H/R = 4. Using reflective flakes to visualise the vortex tubes on the sidewall, they showed that their onset time and wavelength are scalable with Re. These findings have been confirmed, again with reflective flakes, in other high aspect ratio configurations, $H/R > 4$ (Maxworthy, 1972; Mathis and Neitzel, 1985) and computationally in infinitely long cylinders (Neitzel and Davis, 1981; Kaiser et al., 2019). Kim and Choi (2006) have also provided an analytical model which estimates the onset time and associated wavelength in an infinitely long cylinder.

Nevertheless, the behaviour of the sidewall boundary layer after the onset of the vortices, is still not well understood. Euteneuer (1968, 1972) observed that for $1000 < Re < 20000$, the primary vortex pairs grow linearly at the same rate at first, after which they lose their structured shape and begin chaotically rearranging into fewer larger pairs. At this point, to which they refer as 'knick', the vortex wavelength also begins growing at a higher linear rate. Euteneuer (1972) observed that this new growth rate is drastically higher for $Re > 8000$ compared to $Re < 8000$; a phenomenon they explained with the onset of three-dimensional turbulence in an otherwise laminar boundary layer. More recently, the mechanisms through which the flow transitions to turbulence at the moment of 'knick' has been addressed computationally by Kaiser et al. (2019) in an infinitely long cylinder ($3000 < Re < 28000$).

The different transient flows generated within an intermittently rotating cylinder bioreactor are integral to the efficiency of the bioprocess, particularly in the context of CAR-T manufacturing. For example, Amini et al. (2020) showed that agitation plays a fundamental role in the proliferation of primary T-cells. However, in a bioprocessing context, the intermittently rotating cylinder remains largely unstudied, and the implications of the agitation pattern and its impact on mixing, oxygen transfer, solids suspension efficiency, shear stress, and power input remain unknown.

In an earlier study Atanasova et al. (2023) conducted an experimental Particle Image Velocimetry (PIV) and Planar Laser-Induced Fluorescence (PLIF) study, characterising the secondary flow and mixing in a partially filled cylinder (L/R = 0.5) during spin-up and spin-down to rest from solid body rotation. The flow was examined in terms of core flow, boundary layer flow and mixing dynamics. Micromixing was found to mainly occur during spin-down under the effect of the Taylor-Görtler instabilities and potential interaction with Bödewadt boundary layer instabilities, which cause both boundary layers to become turbulent. In contrast, little overall mixing was generated by the stable convective (geostrophic) flow during spin-up. It was found that at $Re > 17500$ a single spin-down step from SBR is sufficient to fully mix the liquid, however the flow is compartmentalised and the inviscid core of fluid, which represents a no-mixing zone, is only fully recirculated on the Ekman timescale, on which the angular velocity of the bulk fluid decays. Micromixing, on the other hand, occurs much faster, provided that the instabilities generated are strong enough, but it is confined to the boundary layers, which expand as the inviscid core retracts.

To the best of the author's knowledge, spin-down to rest has been studied theoretically, experimentally or computationally only when the starting state of the fluid is solid body rotation (SBR). To address this gap in the understanding of the flow mechanics and mixing implications of spin-down to rest in a rotating cylinder bioreactor, this study extends previous work to spin-down starting from different states of the fluid before solid body rotation is reached in the preceding spin-up stage, i.e. spin-down from incomplete spin-up. Novel Particle Image Velocimetry (PIV) and Planar Laser-Induced Fluorescence (PLIF) experiments are presented, shedding light on the effect of increasing spin-up Ekman time, T_{SU}, on the core flow, sidewall boundary layer instabilities and on the mixing in Sections 3.1 – 3.3, respectively. The data presented can be used to inform the design of an intermittent rotation pattern of the CentriCult™, tailored to enhance the mixing and solids suspension performance, the adoption of which would enable higher product yields of the expansion step, ultimately contributing to the collective effort of

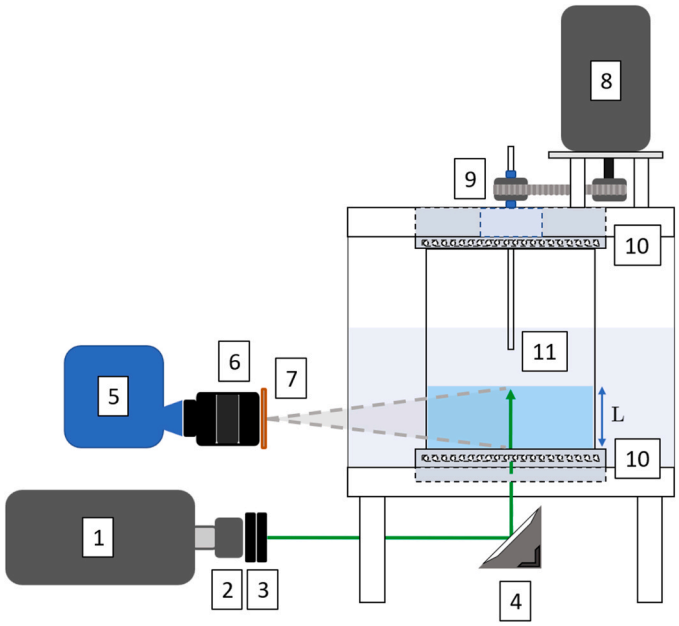

Fig. 2. Experimental setup: 1. Continuous Diode-Pumped Solid-State (DPSS) green laser, 532 nm, 3.6 W (Laserglow Technologies, LRS-0532 Series); 2. Spherical lens; 3. Two cylindrical lenses in series, 25 mm (left) and 15 mm (right); 4. Mirror at 45° to laser sheet; 5. High-speed camera, 7400fps at 1MP (Phantom VEO 710); 6. Micro-NIKKOR 105 mm f/2.8 G IF-ED lens (Nikon); 7. Monochromatic light filter; 8. Low-inertia servo motor (MPL-A320 series, Allen Bradley); 9. Belt-driven rotation mechanism; 10. Ball bearings; 11. Tube for injection of liquids along the vertical axis.

Table 1
Range of operating conditions studied.

Parameter	Range
Ω [rad/s]	π – 3.33π
Ω' [rad/s^2]*	-100π
N [rps]	0.5 – 1.67
Re [-]	7500 – 25000
Fr [-]	0.10 – 1.07
T_{SU} [-]	0.15 – 1.15

* Denotes angular deceleration of the cylinder when its rotation is coming to a stop.

making CAR-T cell therapies more accessible through bioprocess automation.

2. Methodology

A cylindrical plexiglass container with a radius $R = 49$ mm, partially filled with ultrapure water to a liquid height $L = 25$ mm, was used for the experiments to replicate the geometry and aspect ratio of the CentriCult™ bioreactor. The experimental setup is shown in Fig. 2. The cylinder is set in motion by a top mounted motor and is enclosed in a square glass trough to minimise the optical distortion due to refraction at the curved cylindrical wall. The axis of rotation is fixed by two ball bearings, mounted on each cylinder endwall. Table 1 provides a summary of the range of operating conditions that were investigated in this work.

Two-dimensional time-resolved Particle Image Velocimetry (PIV) was used to collect velocity data in the vertical cross-section, bisecting the cylinder, and in the horizontal plane at 18 mm from the bottom ($z/R = 0.37$, $z/L = 0.72$). Neutrally buoyant non-fluorescent polyamide seeding particles with a mean diameter of 5 μm (Dantec Dynamics) were utilised as tracer particles. The fluid was allowed to spin-up for different

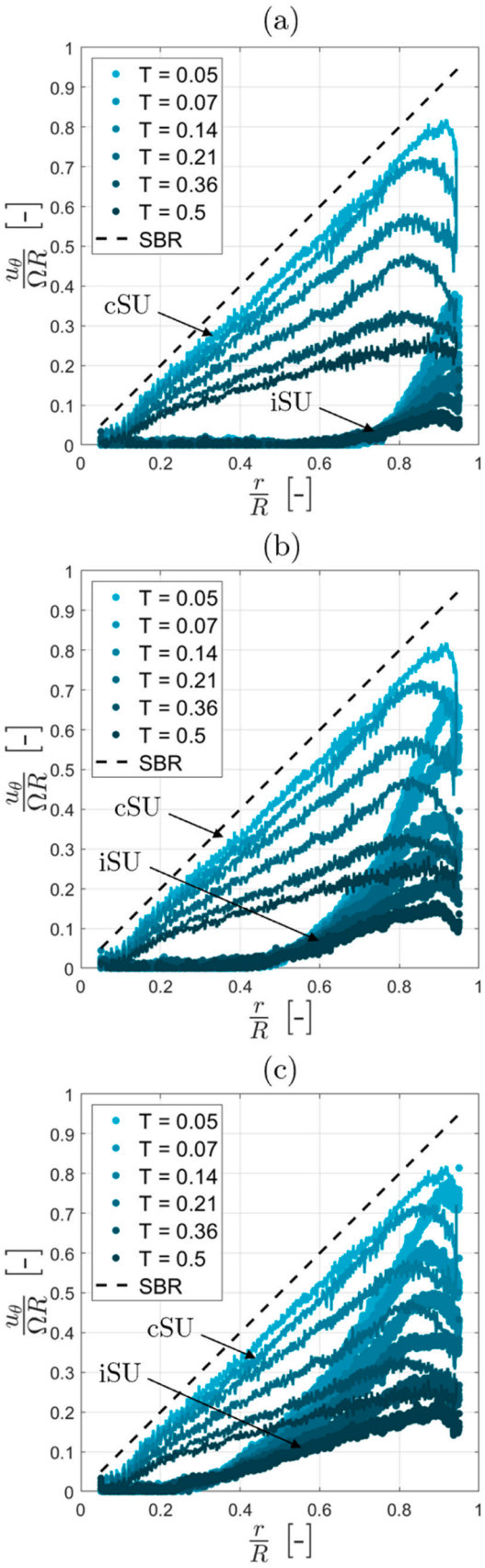

Fig. 3. Instantaneous tangential velocity profiles at z/R = 0.37 Re = 7513) for spin-down to rest after different spin-up times (iSU curves): a) $T_{SU} = 0.13$; b) $T_{SU} = 0.41$; c) $T_{SU} = 0.73$. For reference, the spin-down velocity profiles after complete spin-up are also plotted (cSU curves).

periods of Ekman time, T_{SU}, before the rotation was stopped and the subsequent spin-down stage was analysed. The temporal resolution was varied depending on the Reynolds number and the plane studied, ranging from 0.5 ms for the vertical plane measurements at Re = 7513–1.5 ms for the horizontal plane measurements at $Re = 7513$. The images were processed with an adaptive correlation processing algorithm including a 50 % cell overlap and a final spatial resolution of 8 ×8 pixels, which corresponded to 0.28 mm in the vertical cross-section (3.5 $\times 10^{-5}$ m/px) and to 0.64 mm in the horizontal plane (8 $\times 10^{-5}$ m/px). A cylindrical coordinate system (r, Θ, z) with origin at the centre of the cylinder base was used and the field of view was $r/R = 0 - 0.5$, $z/R = 0 - 0.5$ for the vertical cross-section, and $r/R = 0 - 1$, $\Theta = -90° - 90°$ for the horizontal one.

Planar Laser-Induced Fluorescence (PLIF) was employed in the vertical midplane to visualise the flow and quantify the mixing. A 50 μL drop of a 0.5 mM solution of rhodamine 6 G (Sigma) in ultrapure water was injected at the centre of the bottom endwall prior to the start of rotation. The temporal resolution for different Re was varied from 5 ms (at $Re = 25043$) to 20 ms (at $Re = 7513$), and the spatial resolution was between 4.2 $\times 10^{-5}$ m/px and 8 $\times 10^{-5}$ m/px. The field of view was $r/R = 0 - 1$, $z/R = 0 - 0.5$ for these experiments.

The components of the velocity vector, defined in the cylindrical coordinate system (r, Θ, z) are named u_r, u_θ and u_z.

A reference operating condition of $Re = 7513$ (30 rpm), $Fr = 0.1$, $L/R = 0.5$ was selected for the experiments and is analysed in detail because it features the relevant flow phenomena at higher Re, while also falling in the optimal range of temporal and spatial resolution of PIV.

3. Results and discussion

The results are organised into three subsections. Firstly, the tangential component of the velocity, obtained with PIV, indicative of the core rotational flow, is analysed in Section 3.1 for the reference condition ($Re = 7513$) and for $Re = 17530$. The data is used to establish the scalability of the instantaneous tangential flux during spin-down with the duration of the preceding spin-up stage in Ekman time. In Section 3.2, the study focuses on the sidewall boundary layer and the generation of Taylor-Görtler vortices and turbulence for the reference condition. In Section 3.3, mixing in the bioreactor is studied with PLIF and spin-down from incomplete spin-up is compared to spin-down from solid-body rotation for the reference condition and for $Re = 25043$.

3.1. Core flow

Data is first presented for the reference condition ($Re = 7513$). Profiles of the instantaneous tangential velocity, u_θ, along the radius at height $z/R = 0.37$ ($z/L = 0.72$) are shown in Fig. 3 (with markers) at different Ekman times, T, during spin-down to rest from incomplete spin-up (iSU). The fluid was allowed to spin-up for $T_{SU} = 0.13$ ($t_{SU} = 3.75$ s) in Fig. 3a, for $T_{SU} = 0.41$ ($t_{SU} = 11.63$ s) in Fig. 3b and for $T_{SU} = 0.73$ ($t_{SU} = 20.67$ s) in Fig. 3c, before the rotation was stopped and the resulting spin-down stage was analysed. For comparison, the profiles of u_θ at the same instants in Ekman time, T, obtained for spin-down from solid-body rotation (SBR) are included with solid curves in each subfigure (complete spin-up, cSU). The colour darkens with increasing time. The dashed line indicates the tangential velocity of the fluid at SBR.

Across Fig. 3a-c it is immediately seen that shorter spin-up times than that required to reach SBR result in lower initial tangential velocities at the beginning of spin-down, indicated by the profiles at $T = 0.05$ (markers) compared to those obtained from spin-down from SBR at the same time (solid curves).

It is also seen that for spin-down, following incomplete spin-up, the initial state of the fluid differs from the scenario of spin-down from SBR, discussed in detail in Atanasova et al. (2023). This is seen from the profiles (plotted with markers) in Fig. 3, where the tangential component of the velocity is practically 0 in the interior. At the beginning of

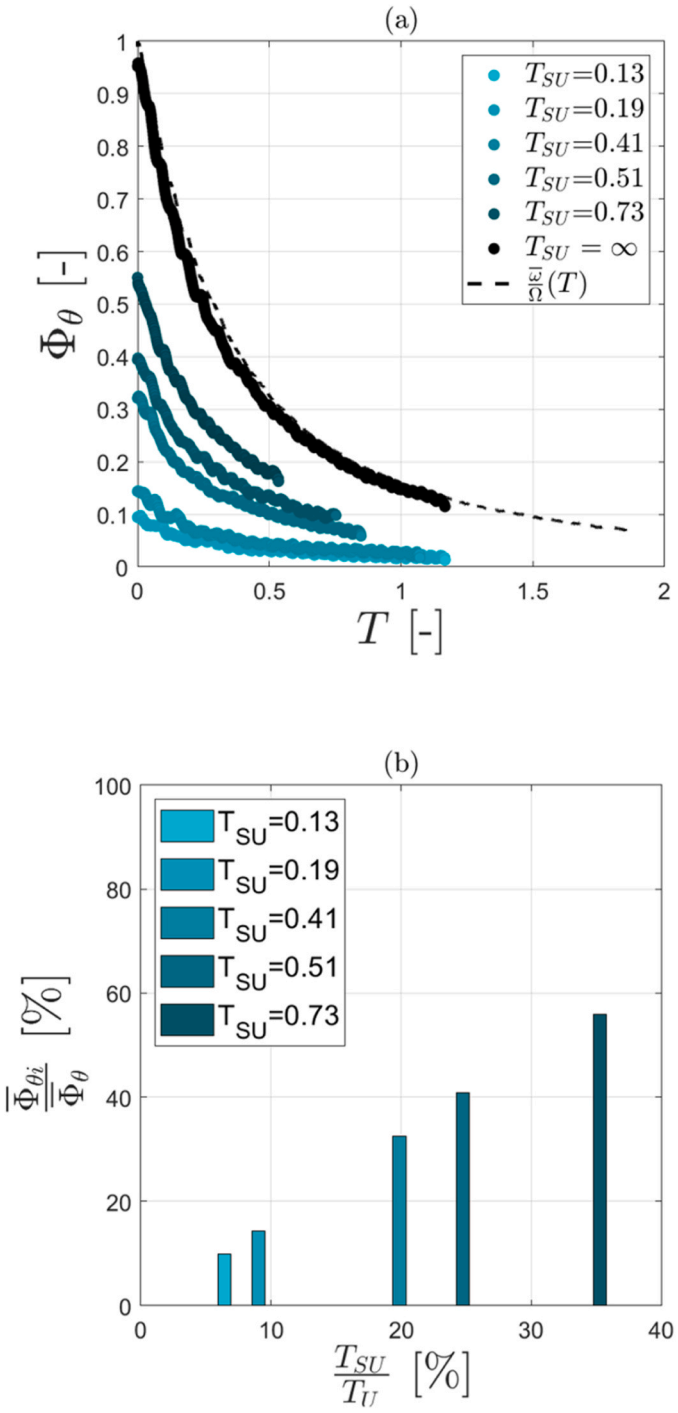

Fig. 4. a) Instantaneous tangential flux at z/R = 0.37 as a function of Ekman time for spin-down after different spin-up times at Re = 7513; b) Ratio of incomplete to complete time-averaged tangential flux, as a function of percentage time spent in the spin-up stage.

spin-down from incomplete spin-up, the inner core of fluid in the cylinder is at rest rather than rotating with a decaying angular velocity as in the case of spin-down from SBR (solid curves). This distinction arises due to the stop of rotation occurring before the propagating shear front, discussed in more detail in Atanasova et al. (2023), has had enough time to reach the axis of rotation during the spin-up process. The front, which propagates radially inward from the sidewall, divides rotating from non-rotating fluid, where fluid ahead of it is at rest. Thus, the longer the spin-up time, the further the front has propagated, and the smaller the

radius is of the inner core of fluid at rest. This effect is clearly visible when comparing analogous instants in Figs. 3a, 2b and 2c.

To show that the radius of the inner non-rotating core at the beginning of spin-down is directly related to the progress of the preceding spin-up stage at the moment of stop of rotation, the radial location, r^*, of the propagating shear front for each of the different levels of incomplete spin-up considered in this section was found from Eq. 3, by substituting the incomplete spin-up times, $T_{SU} = 0.13$, 0.41 and 0.73, respectively. A decay rate coefficient of $b = 1.45$ was used for $Re = 7513$ (Atanasova et al., 2023). Radial positions of the front of $r^*/R = 0.83$, 0.55 and 0.35 were obtained. These are consistent with visual estimates that can be obtained from Figs. 3a – 2c at the first instant, $T = 0.05$ (i.e. the radial position at which the tangential velocity falls below 5 % of the SBR value).

In order to assess the decay of rotation of the fluid in time for spin-down to rest after different spin-up times, and compare the level of rotation acquired by the fluid to that of spin-down from SBR, the instantaneous planar tangential flux, Φ_θ, defined in Eq. 5,

$$\Phi_\theta = \int_0^R \frac{u_\theta}{\Omega R}\frac{dr}{R} \tag{5}$$

was calculated at $z/R = 0.37$ from the tangential velocity profiles shown in Fig. 3 and is plotted against Ekman time in Fig. 4a for five spin-up times: $T_{SU} = 0.13 - 0.73$. The colour darkens with increasing spin-up time, and, for reference, data points from spin-down from SBR (i.e. $T_{SU} = \infty$, complete spin-up) are plotted in black. The dashed curve indicates the decay of angular velocity of the core during spin-down to rest from SBR. This curve was determined experimentally in Atanasova et al. (2023), where the decay of the normalised angular velocity was found to perfectly scale for four different Reynolds number ($Re = 3756$–25043).

As expected, the rate of decay of tangential flux during spin-down from SBR (black markers) is in close agreement with the decay of angular velocity of the core, indicated by the dashed curve for the same (complete spin-up) initial condition. In fact, for this condition the angular velocity of the inviscid core of fluid and the planar tangential flux decay at the same rate and both fall below 5 % of the initial value at Ekman time, $T_D = 2.68$ (Atanasova et al., 2023). The angular velocity of the core could not be estimated for incomplete spin-up conditions since the core is not in rotation. For that reason, the decay of tangential flux is used as an alternative parameter to determine the timescale of spin-down from incomplete spin-up.

For each of the incomplete spin-up conditions the rotation imparted to the fluid is only a fraction of that during spin-down from SBR. The longest spin-up time investigated, $T_{SU} = 0.73$ ($t_{SU} = 20.67$ s), results in initial tangential flux of approximately 57 % of that at solid body rotation, while a spin-up time of $T_{SU} = 0.13$ ($t_{SU} = 3.75$), corresponds to only 10 %. The time-averaged tangential flux, $\overline{\Phi}_{\theta i}$ (the subscript i denotes 'incomplete'), defined in Eq. 6,

$$\overline{\Phi}_{\theta i} = \frac{1}{T}\int_0^\infty \Phi_\theta \quad dT \tag{6}$$

was estimated from each of the incomplete spin-up plots of Fig. 4a and is presented in the bar chart of Fig. 4b as a fraction of the time-averaged tangential flux for spin-down from SBR, $\overline{\Phi}_\theta$. The spin-up Ekman time, T_{SU}, at which the rotation was stopped, is presented as a fraction of the total spin-up time, required to reach solid body rotation, $T_U = 2.08$, (Atanasova et al., 2023). It can thus be seen that spinning up the fluid for 7 % of the time required to reach SBR results in a time-averaged tangential flux of about 10 % that of spin-down from SBR (corresponding to profiles in Fig. 3a). Similarly, a spin-up time of 20 %, results in 36 % of $\overline{\Phi}_\theta$ (corresponding to profiles in Fig. 3b) and a spin-up time of 35 %, in 56 % of the tangential flux at spin-down from SBR (corresponding to profiles in Fig. 3c).

In order to establish the scalability with Re of the tangential momentum imparted to the fluid for different degrees of incomplete spin-

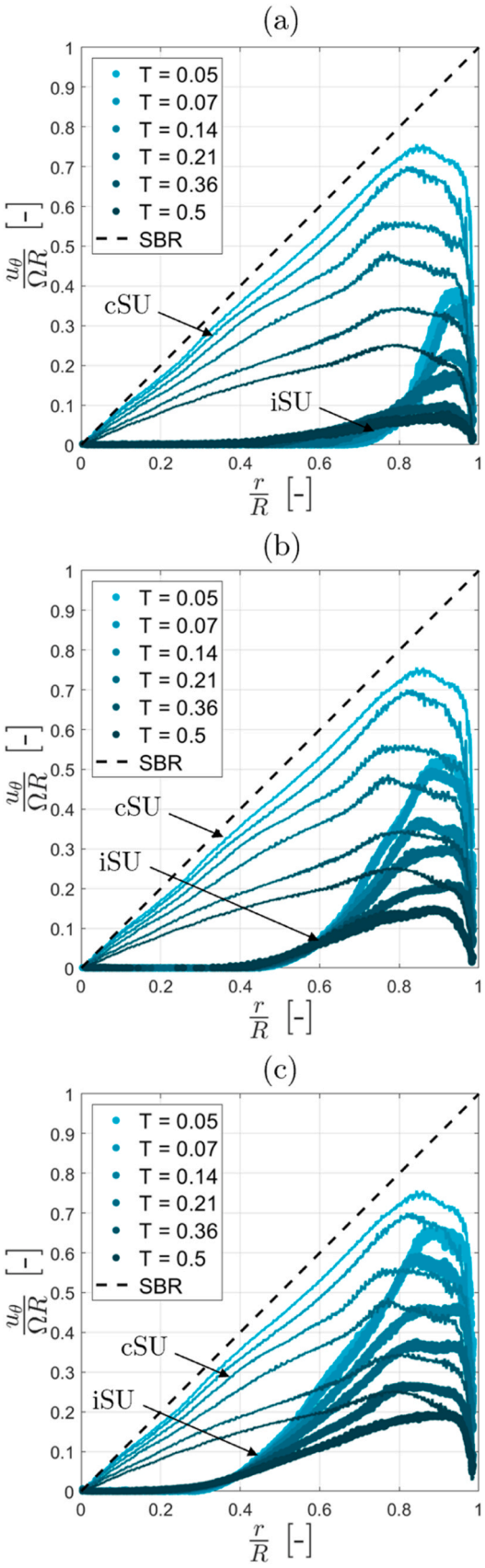

Fig. 5. Instantaneous tangential velocity profiles at z/R = 0.37 Re = 17530) for spin-down to rest after different spin-up times (iSU curves): a) $T_{SU} = 0.15$; b) $T_{SU} = 0.43$; c) $T_{SU} = 0.73$. For reference, the spin-down velocity profiles after complete spin-up are also plotted (cSU curves).

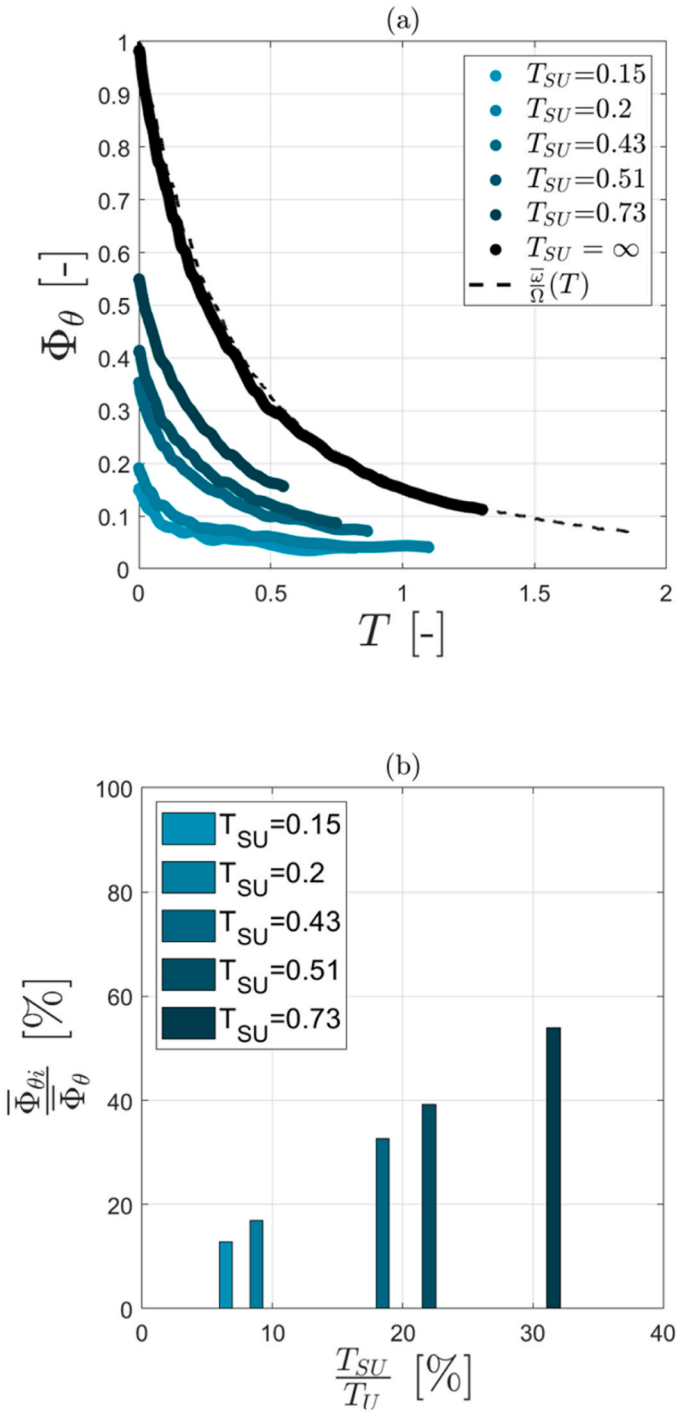

Fig. 6. a) Instantaneous tangential flux, Φ_θ, at z/R = 0.37 as a function of Ekman time for spin-down after different spin-up times at Re = 17530; b) Ratio of incomplete, $\overline{\Phi}_{\theta i}$, to complete time-averaged tangential flux, $\overline{\Phi}_\theta$, as a function of percentage time spent in the spin-up stage.

up, an analogous analysis to that outlined for the reference condition was also carried out for $Re = 17530$. The instantaneous tangential velocity profiles at the same Ekman times after the stop of rotation, T, as in Fig. 3, are included in Fig. 5a, b and c for three similar spin-up Ekman times to those in Fig. 3, $T_{SU} = 0.15$, 0.43 and 0.73 ($t_{SU} = 2.73$, 7.86 and 13.45), respectively.

First of all, it is seen that the spin-down profiles at $Re = 17530$ in Fig. 5 are in very close agreement with those obtained at the reference Re (Fig. 3). For example, for similar spin-up times, similar peaks of non-dimensional tangential velocity are reached and the shapes of the profiles at given T are also comparable between Figs. 3 and 5.

Secondly, it is seen that the shear front, which is formed and propagates during spin-up, continues to diffuse radially inward during spin-down, as the rotating fluid transfers some of its angular momentum to the non-rotating fluid. This is clearly visualised in Fig. 5a, where at the first instant shown, $T = 0.05$, the tangential velocity becomes 0 at $r/R \approx 0.77$, whereas at the latest instant shown, $T = 0.5$, that position has shifted as the front has diffused radially inward, to $r/R \approx 0.45$. While this also occurs at the reference Re, it is not as prominent in Fig. 3a because the dimensional velocities are lower at this regime, and especially in the non-rotating regions, their magnitude is comparable to measurement noise.

Furthermore, the transfer of angular momentum from the rotating to the non-rotating fluid is less prominent for spin-down from higher levels of spin-up (i.e. Fig. 5b, c in comparison to Fig. 5a). This can be explained by considering that the shear stress at the interface between rotating and non-rotating fluid decreases with increasing T_{SU}. This is well visualised by the gradient of the profiles at $T = 0.05$ for the different spin-up times: the steepness of the profile decreases with increasing T_{SU}. This behaviour is to be expected as longer T_{SU} allow more time for the shear front to propagate inward and to lose part of its intensity.

Some deviations are observed in the maxima of the tangential velocity at corresponding instants after the stop of rotation, T, with higher values being reached for the lower Re. This behaviour is more noticeable at higher spin-up times, and for example u_θ reaches values as high as $0.7\Omega R$ and $0.8\Omega R$ at $T_{SU} = 0.41$ and 0.73 for $Re = 7513$ (Fig. 3b and c), while values of $0.5\Omega R$ and $0.65\Omega R$ are obtained at corresponding spin-up times for $Re = 17350$ (Fig. 5b and c). This trend is expected and is in good agreement with the spin-up data presented by Atanasova et al. (2023), where it was shown that the propagating front of the tangential velocity moves faster at lower Reynolds number and Froude number. For example, the latter work showed that the Ekman decay timescale ($1/b$), on which the shear front propagates from the sidewall to the axis of rotation, increases with Fr ($0.02 < Fr < 1.1$) from 0.63 to 0.76, indicating that the spin-up process occurs more slowly in Ekman time at higher Re/Fr.

Therefore, a spin-down process following an incomplete spin-up for a fixed spin-up time will exhibit higher nondimensional momentum/energy levels for lower Re. Furthermore, the peak of tangential velocity during spin-down is also affected by the onset of T-G vortices near the sidewall, which cause the local velocity maxima to decrease and plateau. As outlined by Atanasova et al. (2023), their onset does not scale with Ekman time, but occurs earlier for higher Re, which could further explain the differences observed in the peak tangential velocity obtained between analogous incomplete spin-up profiles of Figs. 3 and 5 at different Reynolds numbers.

Similarly to the analysis carried out for the reference $Re = 7513$ (Fig. 4), the instantaneous tangential flux, Φ_θ, and the time-averaged tangential flux, $\overline{\Phi}_\theta$, are plotted in Fig. 6a and b for $Re = 17530$, respectively. The spin-up Ekman time before the rotation was stopped, T_{SU}, is presented as a percentage of the total Ekman time required to reach SBR at that Re, $T_U = 2.31$ (Atanasova et al., 2023).

By comparing Figs. 6 and 4, it is apparent that both the decay of instantaneous and time-averaged tangential fluxes are in very close agreement between analogous sets of data taken at the two Reynolds numbers with no more than 1.5 % variation. This data seems to indicate that the decay of rotation of the fluid during spin-down from different levels of spin-up is scalable with spin-up Ekman time, T_{SU}, for the range of Re examined and could be used to tailor novel intermittent strategies where a fraction of angular momentum of that obtained with complete spin-up has to be imparted to the fluid.

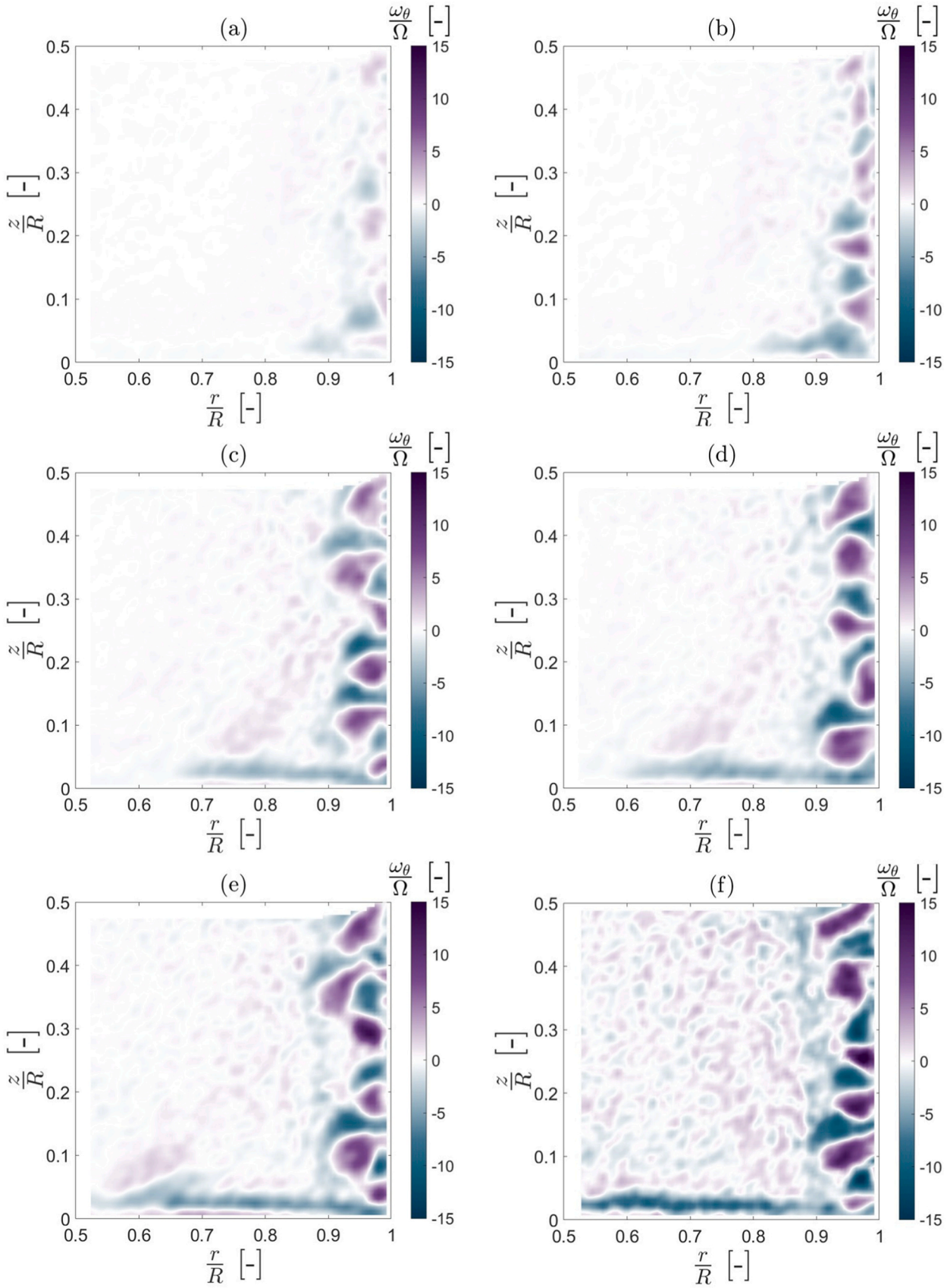

Fig. 7. Instantaneous normalised vorticity, ω_θ/Ω, in the vertical plane for Re = 7513 at Ekman time, T, after the stop of rotation for spin-down after different spin-up times, T_{SU} = 0.12, 0.19, 0.40, 0.51, 0.71; T = 0.100, 0.077, 0.065, 0.063, 0.061 and 0.055, for a) – f) respectively.

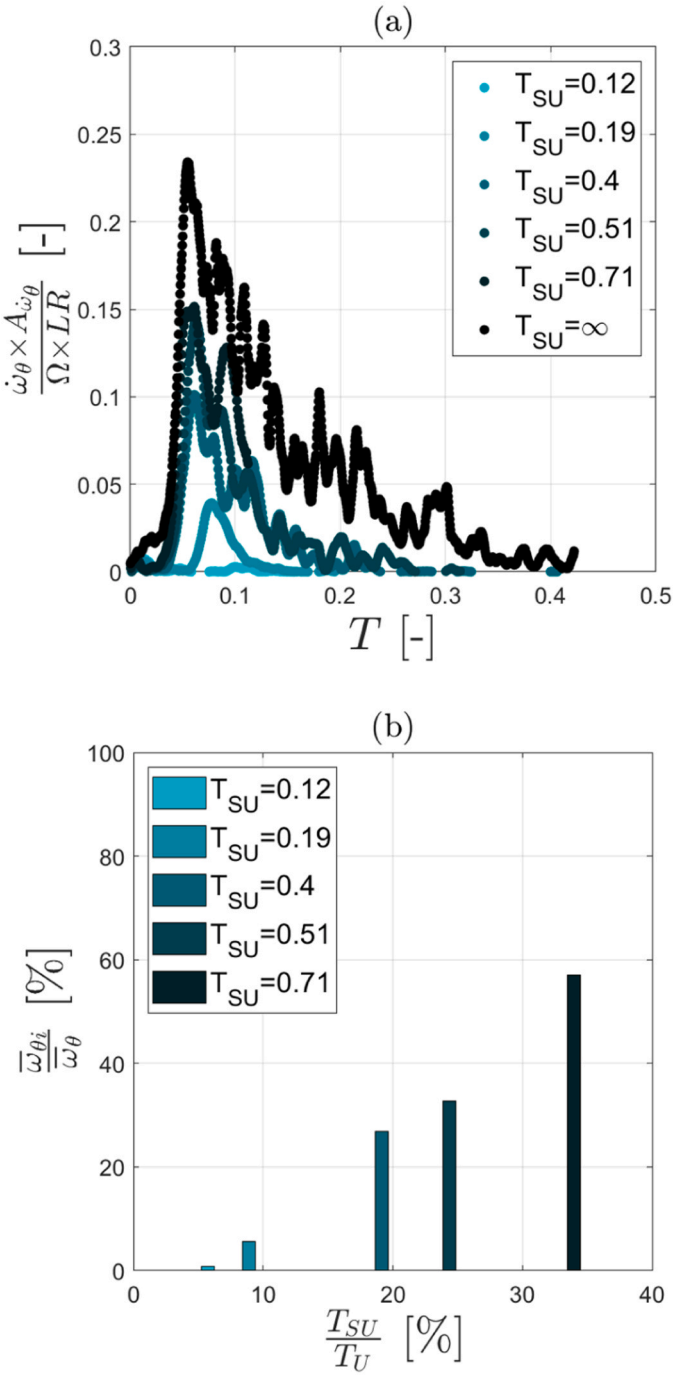

Fig. 8. a) Average instantaneous vorticity in the cross section as a function of Ekman time for different spin-up times at Re = 7513; b) Time-average vorticity for spin-down after different spin-up times, expressed as a fraction of that achieved during spin-down from solid body rotation.

3.2. Sidewall boundary layer

The following section focuses on the generation of Taylor-Görtler (T-G) vortices during spin-down from incomplete spin-up. PIV results obtained in the vertical cross-section are presented, quantifying the vorticity of the T-G instabilities.

Fig. 7 shows a contour plot of the instantaneous normalised tangential vorticity in the vertical cross section, ω_θ/Ω, for spin-down from incomplete spin-up, $T_{SU} = 0.12, 0.19, 0.40, 0.51, 0.71$ in Fig. 7a – e, respectively, and for spin-down from SBR in Fig. 7f (reference condition, $Re = 7513$). The instants in Ekman time illustrated are $T =$ 0.100, 0.077, 0.065, 0.063, 0.061 and 0.055 for Fig. 7a – f, respectively.

It is immediately seen that the size of the vortex pairs formed is roughly the same for all experimental conditions shown in Fig. 7, however shorter spin-up times lead to later onset and lower non-dimensional vorticity magnitude of the corresponding T-G vortices. This behaviour is to be expected since T-G vortices are generated by the instantaneous deceleration of the flow in the boundary layer at the curved sidewall, and therefore their intensity depends on the amount of tangential flux imparted to the fluid during the preceding spin-up stage. In Fig. 7a, it is seen that the shortest spin-up time, $T_{SU} = 0.12$, results in the generation of only two vortex pairs (in proximity to the horizonal midplane and close to the bottom at $z/R \approx 0.25$ and 0.05, respectively) of very low vorticity magnitude (i.e. $\omega_\theta/\Omega < 2$. For the second lowest spin-up time, $T_{SU} = 0.19$, two structured pairs are present near the lower half of the sidewall, while more pairs are in the process of forming in the upper part of the sidewall closer to the surface. For these two spin-up times, the vortices formed were observed to grow in time, as their vorticity decayed, without losing their coherent structure. For all the other spin-up times, $T_{SU} \geq 0.40$, the full number of vortex pairs, i.e. 4–5, expected at $Re = 7513$ was observed (see Fig. 7c – f), and their transition to turbulence occurred similarly to spin-down from SBR.

To compare the intensity and decay timescale of the T-G instabilities between spin-down from different degrees of incomplete spin-up, a similar analysis was carried out on the vorticity data as that outlined in Atanasova et al. (2023). The λ_2 technique with a threshold of $\lambda_2 = -6.5\left(\frac{2\Omega}{\pi}\right)^2$ was employed to differentiate the vorticity generated by the T-G instabilities from local gradients due to experimental noise. The total instantaneous vorticity in the plane was found by multiplying the in-plane average vorticity of the T-G instabilities, $\dot{\omega}_\theta$, by the area of the corresponding cross-section, $A_{\dot{\omega}_\theta}$. The resulting curves are shown in Fig. 8a for the different spin-up times studied ($T_{SU} = 0.12 – 0.71$) at the reference condition ($Re = 7513$). The colour darkens with increasing spin-up time, while spin-down from SBR ($T_{SU} = \infty$) is plotted in black.

From Fig. 8a it is seen that the total instantaneous vorticity in the plane is 0 at the beginning of spin-down. It then increases sharply due to the onset of the T-G vortices and peaks shortly after the stop of rotation. It should be noted that the instants in time illustrated in each subplot in Fig. 7 ($T = 0.100, 0.077, 0.065, 0.063, 0.061$ and 0.055 for Fig. 7a – f, respectively) correspond to the moment at which the total instantaneous vorticity plotted in Fig. 8a peaks for that experimental condition. This instant was identified by Atanasova et al. (2023) as the moment of 'knick', described by Euteneuer (1972) and Kaiser et al. (2019) and corresponds to the last time the T-G vortices are seen as structured pairs before they transition to turbulence. In agreement with Fig. 7, the vorticity of the T-G instabilities is barely detectable and remains close to 0 for the shortest spin-up time studied, $T_{SU} = 0.12$. Similarly, the second shortest spin-up time, $T_{SU} = 0.19$, at which also fewer pairs were produced, yields a very low vorticity peak, around 15 % of the peak for spin-down from SBR. To quantify the total vorticity of the T-G vortices for a given spin-down process, the integral of the total vorticity in time, $\overline{\omega}_{\theta i}$, defined in Eq. 7,

$$\overline{\omega}_{\theta i} = \int_0^\infty \frac{\dot{\omega}_\theta A_{\dot{\omega}_\theta}}{\Omega LR} \, dT \tag{7}$$

was estimated for each incomplete spin-up condition in Fig. 8a and is plotted as a fraction of the integral of the total vorticity in time of spin-down from SBR, $\overline{\omega}_\theta$, in the bar chart of Fig. 8b. Analogously to Fig. 4b, the spin-up time is expressed as a percentage of the total spin-up time required to reach solid body rotation at the corresponding Re (i.e. $T_U = 2.08$ at $Re = 7513$, see Atanasova et al., 2023). The integral of the total vorticity of the T-G instabilities in time, generated after the shortest spin-up time, $T_{SU} = 0.12$, is merely 1 % of that produced by spin-down from solid-body rotation, while the time-averaged tangential flux yielded by a very similar spin-up time, $T_{SU} = 0.13$, was 10 % (see Fig. 4b). Similarly, a time-averaged tangential flux of 13 % ($T_{SU} = 0.19$)

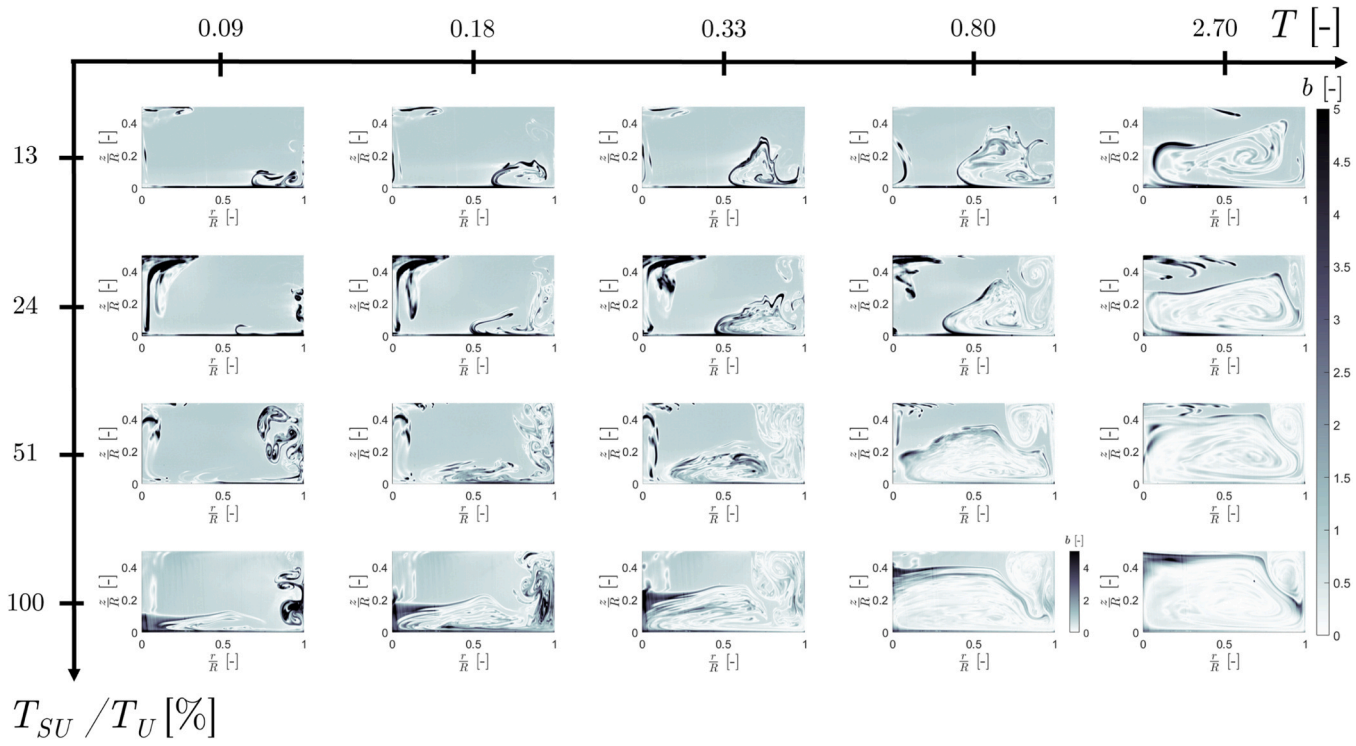

Fig. 9. Normalised instantaneous pixel brightness, b, obtained with PLIF in the vertical cross-section for spin-down from incomplete spin-up at Re = 7513; The x-axis shows the spin-down Ekman time, T, and the y-axis depict different spin-up times, T_{SU}, as percentage of the Ekman time required to reach SBR.

corresponds to only 6 % of the integral of the total vorticity in time of spin-down from SBR. For those two conditions, the T-G vortices formed did not transition to turbulence and fewer pairs were observed (ref to Fig. 7). However, with the higher spin-up times, $T_{SU} \geq 0.4$, the percentage of $\overline{\omega}_\theta$ achieved is much closer to the percentage of time-averaged tangential flux achieved for a given spin-up time. The best agreement is observed at the highest spin-up time, where $\overline{\omega}_{\theta i}/\overline{\omega}_\theta =$ 57 % ($T_{SU} = 0.71$, Fig. 8b) and $\overline{\Phi}_{\theta i}/\overline{\Phi}_\theta = 56$ % ($T_{SU} = 0.73$, Fig. 4b). This data indicates that to achieve a reasonable level of convective flow within the bioreactor, and at the same time obtain more intense vortices promoting local mixing, spin-up Ekman times higher than 0.5 should be considered.

3.3. Mixing study

Complementary to the PIV experiments presented in Sections 3.1 and 3.2, PLIF was employed as a technique to gain insight into the mixing dynamics during spin-down from incomplete spin-up.

Fig. 9 illustrates instantaneous PLIF data at Ekman times, T, after the stop of rotation (abscissa) for spin-down after different spin-up times, T_{SU} (ordinate), expressed as a percentage of the Ekman spin-up time required to reach SBR, T_U, at the reference condition ($Re = 7513$). The last row illustrates the spin-down from complete spin-up (i.e. from SBR). The colormap shows the normalised pixel brightness, b, as defined in Eq. 8,

$$b = \left| \frac{M - M_1}{M_1 - M_0} \right|, \tag{8}$$

where M is the value of the instantaneous brightness of a pixel, which can vary between 0 and 65535. M_0 is the value of the pixel brightness before the injection of dye, and M_1 refers to the final brightness when the dye is completely mixed. Pixels which have achieved the final value of brightness, M_1, are completely mixed and appear in white hues in Fig. 9 ($b = 0$). On the other hand, pixels with concentrated dye appear dark, while pixels with no dye (i.e. $M = M_0$) are characterised by $b = 1$.

In Fig. 9 it is immediately seen that there is a significant improvement in the mixing during spin-down with increasing duration of the preceding spin-up stage, which is to be anticipated as the intensity of the T-G vortices, contributing to local fine-scale mixing, is directly dependent on the spin-up time, as shown in Fig. 7. As expected, spin-down from SBR results in the most homogenous distribution of the dye at $T = 2.70$ (last column of Fig. 9), when the fluid has practically come to rest, i.e. > 95 % of the tangential flux has been dissipated (ref. to Fig. 6). Similarly to spin-down from SBR, three distinct regions of the flow can be identified for spin-down from incomplete spin-up: the sidewall boundary layer (right side), where the T-G instabilities decay and contribute to local mixing, the endwall boundary layer (bottom), which is dominated by the (clockwise) Ekman circulation, visualised by the dark strip of dye, and the inviscid interior with no dye (top-left side). However, it is seen that for spin-down from incomplete spin-up, the Ekman circulation, which is responsible for recirculating the fluid micromixed in the boundary layers across the volume of the cylinder, does not extend to the full cylinder radius but instead is limited to the corner of the cylinder for $T_{SU}/T_U = 13$ % and 24 %, while fluid near the bottom at inner radii remains free of dye. It is also seen that by the time spin-down is completed (i.e. $T = 2.7$), the Ekman layer has not expanded all the way to the free surface for any of the incomplete spin-up conditions, leaving fluid near the surface unmixed, while for spin-down from SBR, the Ekman convection has recirculated the entire volume of fluid.

To quantify the mixing efficiency of the different spin-up times illustrated in Fig. 9, the fraction of mixed pixels (i.e. pixels which have achieved the final value of brightness, M_1) from the total number of pixels in the cross-section, γ_M, was plotted for the reference condition ($Re = 7513$) in Fig. 10a and for a higher Reynolds number, $Re = 25043$, in Fig. 10b. Analogously to Atanasova et al. (2023), a pixel is considered mixed when $b < 0.4$. The dashed curve provides a reference line for the spin-down process from solid body rotation ($T_{SU} = \infty$) at each Re. In Fig. 10a, the grey gradient illustrates the decay of vorticity of the T-G vortices across the range of T_{SU} considered, obtained from Fig. 8a, and darker hues indicate longer spin-up times. A grey band to refer to the

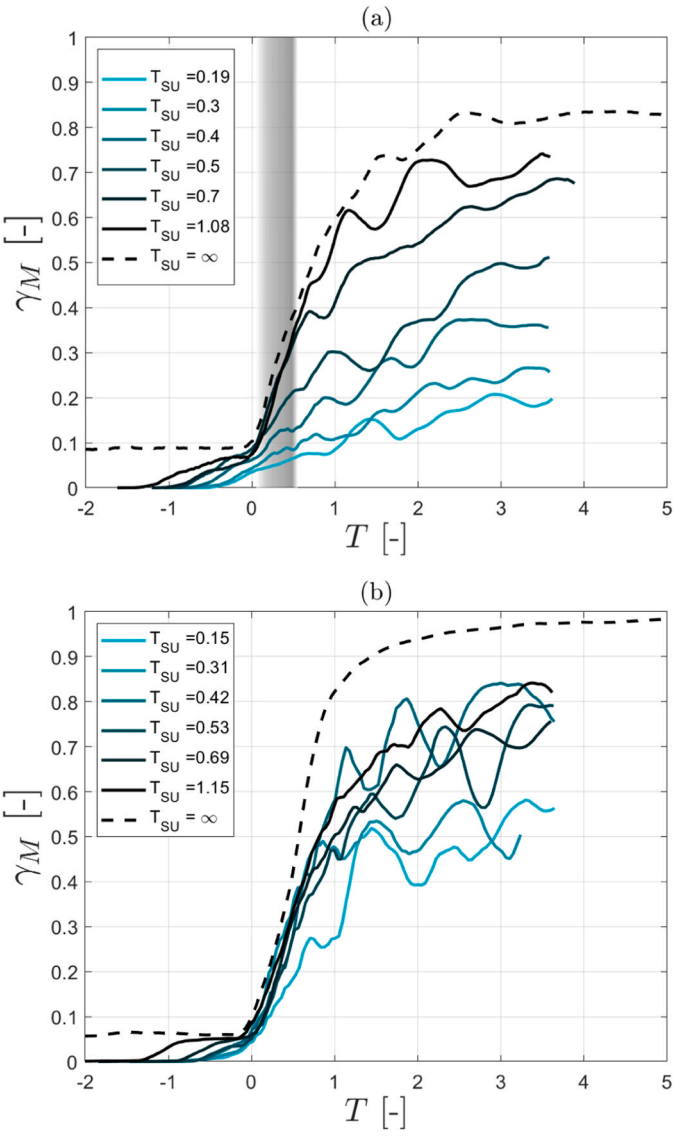

Fig. 10. Fraction of mixed pixels from the total number of pixels in the cross-section, showing the rate of macromixing for spin-down to rest after different spin-up times for Re = 7513 and 25043 in a) and b), respectively. The dashed curve shows the rate of macromixing for spin-down from SBR.

onset and decay of the T-G vortices is not included in Fig. 10b, as the limit of temporal and spatial resolution of PIV did not allow to resolve their scale at this Reynolds number (Re = 25043). However, from vorticity decay data at different Re provided in Atanasova et al. (2023), it can be anticipated that the T-G vortices would last longer than those at the lower Reynolds number.

A trend of increasing mixing efficiency of the spin-down process with increasing spin-up times is clearly visible for both Re. For the reference condition (Fig. 10a), the shortest spin-up time (T_{SU} = 0.19), results in less than 20 % of the fluid being mixed by the time rotation has fully decayed (T_D = 2.68). This spin-up time was related to time-averaged tangential flux of 13 % and integral of the total vorticity in time of only 6 % of those achieved for spin-down from SBR. On the other hand, a spin-up time, T_{SU} = 1.08 (T_{SU}/T_U = 52 %), resulted in about 70 % of the fluid being mixed, which tends towards the level of mixing achieved for spin-down from SBR at this Re, $\gamma_M \approx$ 80 %. At the higher Re studied, Fig. 10b, it is noticed that similar spin-up times lead to overall better mixing with the lowest T_{SU} = 0.15, resulting in $\gamma_M \approx$ 45 %, as opposed to $\gamma_M \approx$ 20 % for T_{SU} = 0.19 at the reference condition (Fig. 10a). This could be attributed to the overall higher vorticity, smaller scale of instabilities and longer vorticity decay timescales at the higher Re. An interesting observation is that while the trend of improved mixing with longer spin-up times is maintained, the variation of the level of mixing with T_{SU} is smaller at Re = 25043 than at the reference Re, as spin-up times of $0.42 < T_{SU} < 1.15$ all lead to 65–75 % of the fluid being mixed at $T = T_D = 2.68$. This points to fact that when the spin-up stage of the rotation pattern of the bioreactor is incomplete, higher rotation speeds should be considered for the following spin-down stage to yield optimal mixing, however this may come at the expense of increased shear stress and power consumption. The large oscillations in the level of mixing, for both Figs. 10a and 10b, could be attributed to patches of dye, periodically passing through the laser plane as the rotation of the fluid decays.

4. Conclusions

The transient flow during spin-down to rest from solid body rotation (SBR) in a cylinder has been previously characterised by several works in different disciplines, however, from a bioprocessing perspective, the flow remains largely unstudied, and the implications of the rotation pattern of the intermittently rotating cylinder bioreactor (i.e. the CentriCult™) for mixing, oxygen transfer, solids suspension, shear stress, and power input remain unknown. Moreover, spin-down has only been addressed in the literature when the starting state of the fluid is solid body rotation. The present study offers novel PIV and PLIF data and provides insight into the fluid dynamics during spin-down to rest, starting from different states of the fluid before solid body rotation is reached in the preceding spin-up stage, i.e. spin-down from incomplete spin-up, which is the current *modus operandi* of the CentriCult™.

The influence of spin-up Ekman time, T_{SU}, on the core flow, the Taylor-Görtler (T-G) instabilities, and on the mixing dynamics was investigated. It was found that shorter spin-up times than those required to reach SBR lead to lower tangential flux during spin-down, which is a fixed fraction of that during spin-down from SBR and scales with the spin-up Ekman time at the two Re examined: Re = 7500 and 17500. The inner core of fluid, located inward of the propagating shear front of tangential velocity, i.e. at $r < r^*(T_{SU})$, is at rest, rather than subject to SBR with decaying angular velocity at the beginning of spin-down. The outer fluid, which is rotating, transfers some of its angular momentum, by viscous diffusion, to the fluid at rest as the rotation decays on the convective Ekman timescale.

Furthermore, Taylor-Görtler (T-G) vortices were observed for spin-down from incomplete spin-up, for the range of T_{SU} examined (0.12 – 0.71) at the reference condition, Re = 7500. However, their vorticity was lower, and they decayed sooner for shorter spin-up times. The time-averaged vorticity achieved was calculated as a fraction of the time-averaged vorticity for spin-down to rest. It was observed that for spin-up times 0.12 and 0.19, not all T-G vortex pairs formed, and they did not transition to turbulence. This resulted in very low time-averaged vorticity of 1 % and 6 %, respectively, of that achieved during spin-down from SBR. On the other hand, with longer spin-up times, $T_{SU} >$ 0.4, the full array of T-G vortices was generated, and the integral of the total vorticity in time scaled fairly well with the time-averaged tangential flux for the range of spin-up times studied (0.4 – 0.71).

The mixing efficiency of spin-down from incomplete spin-up was investigated for the reference condition and for a higher Re of 25000. Mixing was found to improve with longer spin-up durations, approaching a mixing time closer to that for spin-down from SBR with spin-up times, $T_{SU} > 1$. However due to the lower intensity of the T-G instabilities, none of the incomplete spin-up conditions tested ($0.15 < T_{SU} > 1.15$) resulted in complete mixing. Therefore, spinning up the fluid to SBR before initiating spin-down is more beneficial for homogenisation in the bioreactor but also results in increased shear stress and power consumption due to the higher tangential velocity and stronger vorticity of the T-G instabilities.

Finally, it is worth to mention that while longer spin-up times result in an improvement in the micromixing during spin-down due to the higher intensity and duration of the T-G vortices, macromixing is still limited by the convective Ekman timescale, on which rotation decays as the fluid is recirculated through the endwall boundary layer. To avoid this limitation, the rotation pattern of the cylinder must be designed in such a way that generates flow which disrupts the interior fluid early on, so that the enhanced mixing due to turbulence is not confined to the boundary layers. This is the focus of future work where spin-over will be examined as an alternative rotation step in the intermittent agitation pattern of the bioreactor.

CRediT authorship contribution statement

G.G.Atanasova: Conceptualization, Data curation, Formal analysis, Investigation, Writing – original draft, Writing – review & editing. **A. Ducci:** Conceptualization, Investigation, Resources, Supervision, Writing – review & editing. **M.Micheletti:** Funding acquisition, Supervision, Writing – review & editing.

Declaration of Competing Interest

The authors declare that they have no known competing financial interests or personal relationships that could have appeared to influence the work reported in this paper.

Acknowledgements

Funding from the UK Engineering & Physical Sciences Research Council (EPSRC) for the Future Targeted Healthcare Manufacturing Hub hosted at University College London with UK university partners is gratefully acknowledged (Grant Reference: EP/P006485/1).Financial and in-kind support from the consortium of industrial users and sector organisations is also acknowledged.

References

Alzubi, J., Lock, D., Rhiel, M., Schmitz, S., Wild, S., Mussolino, C., Hildenbeutel, M., Brandes, C., Rositzka, J., Lennartz, S., Haas, S.A., Chmielewski, K.O., Schaser, T., Kaiser, A., Cathomen, T., Cornu, T.I., 2021. Automated generation of gene-edited CAR T cells at clinical scale. Mol. Ther. Methods Clin. Dev. 20, 379–388.

Amini, A., Wiegmann, V., Patel, H., Veraitch, F., Baganz, F., 2020. Bioprocess considerations for T-cell therapy: investigating the impact of agitation, dissolved oxygen, and pH on T-cell expansion and differentiation. Biotechnol. Bioeng. 117 (10), 3018–3028.

Atanasova, G.G., Micheletti, M., Ducci, A., 2023. Fluid flow and mixing in a novel intermittently rotating bioreactor for CAR-T cell therapy manufacturing. Chem. Eng. Sci. 281.

Cappell, K.M., Kochenderfer, J.N., 2023. Long-term outcomes following CAR T cell therapy: what we know so far. Nat. Rev. Clin. Oncol.

Chaudhuri, J.B., Al-Rubeai, M., 2005. Bioreactors for Tissue Engineering. Springer.

Choi, S., Kim, J.W., Hyun, J.M., 1989. Transient free surface shape in an abruptly rotating, partially filled cylinder. J. Fluids Eng. 111 (4), 439–442.

Choi, S., Kim, J.W., Hyun, J.M., 1991. Experimental investigation of the flow with a free surface in an impulsively rotating cylinder. J. Fluids Eng. 113 (2), 245–249.

Cogan, S.J., Ryan, K., Sheard, G.J., 2011. The effects of vortex breakdown bubbles on the mixing environment inside a base driven bioreactor. Appl. Math. Model. 35 (4), 1628–1637.

Cui, X., 2004. Numerical simulations of the generation of Taylor–görtler vortices during spin-down to rest in finite-length cylinders. Comput. Fluids 33 (4), 603–621.

Curran, S.J., Black, R.A., 2004. Quantitative experimental study of shear stresses and mixing in progressive flow regimes within annular-flow bioreactors. Chem. Eng. Sci. 59 (24), 5859–5868.

Curran, S.J., Black, R.A., 2005. Oxygen transport and cell viability in an annular flow bioreactor: comparison of laminar couette and Taylor-vortex flow regimes. Biotechnol. Bioeng. 89 (7), 766–774.

Duck, P., Foster, M., 2001. Spin-Up of homogeneous and stratified fluids. Annu. Rev. Fluid Mech. 33, 231–263.

Dusting, J., Balabani, S., 2009. Mixing in a taylor-couette reactor in the non-wavy flow regime. Chem. Eng. Sci. 64 (13), 3103–3111.

Dusting, J., Sheridan, J., Hourigan, K., 2006. A fluid dynamics approach to bioreactor design for cell and tissue culture. Biotechnol. Bioeng. 94 (6), 1196–1208.

El-Khazragy, N., Ghozy, S., Emad, P., Mourad, M., Razza, D., Farouk, Y.K., Mohamed, N. A., Ahmed, M.K., Youssef, T., Bahnasawy, Y.M., Elmasery, S., 2020. Chimeric antigen receptor T cells immunotherapy: challenges and opportunities in hematological malignancies. Immunotherapy.

Euteneuer, G., 1968. Störwellenlängen-messung bei längswirbeln in laminaren grenzschichten an konkav gekrümmten wänden. Acta Mech. 7, 161–168.

Euteneuer, G., 1972. Die entwieklung von längswirbeln in zeitlich anwachsenden grenzschichten an konkaven wänden. Acta Mech. 13, 215–223.

Floryan, J.M., 1991. On the görtler instability of boundary layers. Prog. Aerosp. Sci. 28 (3), 235–271.

Goller, H., Ranov, T., 1968. Unsteady rotating flow in a cylinder with a free surface. J. Basic Eng. 90, 445–454.

Goller, H., Ranov, T., 2013. Discussion with Benton and Greenspan, 17 (February), 2013.

Greenspan, H.P., 1968. The Theory of Rotating Fluids. Cambridge University Press.

Greenspan, H.P., Howard, L.N., 1963. On a time-dependent motion of a rotating fluid. J. Fluid Mech. 17 (3), 385–404.

Gustafson, M.P., Ligon, J.A., Bersenev, A., McCann, C.D., Shah, N.N., Hanley, P.J., 2022. Emerging frontiers in immuno- and gene therapy for cancer. Cytotherapy.

Homicz, G., Gerber, N., 1987. Numerical model for fluid spin-up from rest in a partially filled cylinder. J. Fluids Eng. 109, 194–197.

Kaiser, F., Frohnapfel, B., Ostilla-Mónico, R., Kriegseis, J., Rival, D.E., Gatti, D., 2019. On the stages of vortex decay in an impulsively stopped, rotating cylinder. J. Fluid Mech.

Kim, M.C., Choi, C.K., 2006. The onset of taylor-görtler vortices during impulsive spin-down to rest. Chem. Eng. Sci. 61, 6478–6485.

Kloosterziel, R.C., Van Heijst, G.J.F., 1992. The evolution of stable barotropic vortices in a rotating free-surface fluid. J. Fluid Mech. 239, 607–629.

Lopez, J.M., Marques, F., Rubio, A.M., Avila, M., 2009. Crossflow instability of finite bödewadt flows: transients and spiral waves. Phys. Fluids 21 (11), 1–9.

Mathis, D.M., Neitzel, G.P., 1985. Experiments on impulsive spin-down to rest. Phys. Fluids 28 (2), 449–454.

Maxworthy, T., 1972. The structure and stability of vortex rings. J. Fluid Mech. 51, 15–32.

Mock, U., Nickolay, L., Philip, B., Cheung, G.W.K., Zhan, H., Johnston, I.C.D., Kaiser, A. D., Peggs, K., Pule, M., Thrasher, A.J., Qasim, W., 2016. Automated manufacturing of chimeric antigen receptor T cells for adoptive immunotherapy using CliniMACS prodigy. Cytotherapy 18 (8), 1002–1011.

Moutsatsou, P., Ochs, J., Schmitt, R.H., Hewitt, C.J., Hanga, M.P., 2019. Automation in cell and gene therapy manufacturing: from past to future. Biotechnol. Lett. 41 (11), 1245–1253.

Munk, W., 2001. Spirals on the sea. Sci. Mar. 65, 193–198.

Neitzel, G.P., Davis, S.H., 1981. Centrifugal instabilities during spin-down to rest in finite cylinders. numerical experiments. J. Fluid Mech. 102, 329–352.

O'Donnell, J., Linden, P.F., 1991. Free-surface effects on the spin-up of fluid in a rotating cylinder. J. Fluid Mech. 232 (439), 439–453.

Richter, A., 2014. Surmounting the developmental challenges of miltenyi's prodigy cell separation system - an integrated, closed-system cell processing device. 8th Tech. Meet. Adv. Ther. Med. Prod. Manuf. Community.

Saini, S., Wick, T.M., 2003. Concentric cylinder bioreactor for production of tissue engineered cartilage: effect of seeding density and hydrodynamic loading on construct development. Biotechnol. Prog. 19 (2), 510–521.

Saini, S., Wick, T.M., 2004. Effect of low oxygen tension on tissue-engineered cartilage construct development in the concentric cylinder bioreactor. Tissue Eng. 10 (5–6), 825–832.

Schlichting, H., Gersten, K., 2017. Boundary-Layer Theory, 9th ed. Springer, Berlin.

Wedemeyer, E.H., 1964. The unsteady flow within a spinning cylinder. J. Fluid Mech. 20 (3), 383–399.

Zhu, F., Shah, N., Xu, H., Schneider, D., Orentas, R., Dropulic, B., Hari, P., Keever-Taylor, C.A., 2018. Closed-system manufacturing of CD19 and dual-targeted CD20/19 chimeric antigen receptor T cells using the CliniMACS Prodigy device at an academic medical center. Cytotherapy 20 (3), 394–406.